

Precision Υ Spectroscopy and Fundamental Parameters From NRQCD

The NRQCD Collaboration *

We present results from a high precision NRQCD simulation of the quenched Υ system at $\beta = 6$. We demonstrate a variety of important lattice techniques, including the perturbative improvement of actions, tadpole improvement, and multicorrelated fits for extracting the spectrum of excited states. We present new determinations of $\alpha_s(M_Z)$ and M_b , two fundamental parameters of the Standard Model.

1. Introduction

In this paper we report new results from an accurate numerical simulation of the spectrum of the Υ family of mesons. (Results for the J/ψ family are presented in [1].) Our simulation uses the NRQCD [2] action for the quarks, including all relativistic effects through $\mathcal{O}(M_b v^4)$ where M_b is the b -quark's mass and v its average velocity. We demonstrate a variety of important lattice techniques, including the perturbative improvement of actions, tadpole improvement, and multicorrelated fits for extracting the spectrum of excited states. Furthermore, the high statistics and small systematic errors of our results allow us to extract accurate values for two of the fundamental parameters of the Standard Model: the mass of the b -quark, and the strong coupling constant $\alpha_{\overline{\text{MS}}}(M_Z)$.

The b -quarks in Υ 's are quite nonrelativistic (v^2 is about 0.1). We exploit this in NRQCD by replacing the Dirac action for the quarks with a Schrödinger action. The Schrödinger theory is computationally much easier to solve because it can be treated as an initial-value problem, rather than a boundary-value problem. Relativistic effects are systematically introduced, order-by-order in v^2 , as corrections to the nonrelativistic action [2,3]. These terms are quite similar in form to the corrections that remove finite-lattice-spacing errors. We include both types of correc-

tion in our simulations. Consequently the dominant source of systematic error in our results is the gluon action—we use configurations produced with the standard Wilson action, and no light-quark vacuum polarization. (Finite volume errors are negligible since Υ 's are much smaller than ordinary mesons.)

A complication in using improved actions such as ours is that each of the correction terms has its own coupling constant. These new coupling constants must be computed somehow. In principle they can be computed using weak-coupling perturbation theory[2,3]. Our simulations demonstrate that this is also the case in practice, provided tadpole-improved perturbation theory is employed. Indeed (tadpole-improved) tree-level perturbation theory seems quite sufficient for most aspects of Υ physics, at least at $\beta = 6$; and work has begun on the first-order corrections[4]. This perturbative control over the effective action means that there are really only two parameters in the quark action, the mass and the charge, just as in the continuum theory. Thus our simulations are truly calculations from first principles, unlike calculations based upon a QCD-motivated phenomenological model like the quark potential model.

In what follows, we first summarize the details of the simulation and fitting procedures. We then focus upon results for the spectrum, a^{-1} , M_b , and $\alpha_{\overline{\text{MS}}}(M_Z)$. Finally we comment upon the implications of our work concerning improved actions and simulations on coarse grids.

*Based on posters presented by G.P. Lepage and J. Sloan. Members of the collaboration are C.T.H. Davies and A. Lidsey, Univ. of Glasgow; K. Hornbostel, SMU; A. Langnau and G.P. Lepage, Cornell Univ.; C. Morningstar, Univ. of Edinburgh; J. Shigemitsu, Ohio State Univ.; and J. Sloan, Florida State Univ.

2. The Simulation

The NRQCD quark lagrangian we used in our simulations was [3]

$$\psi^\dagger \left(1 - \frac{aH_0}{2n}\right)^n U_4^\dagger \left(1 - \frac{aH_0}{2n}\right)^n (1 - a\delta H) \psi, \quad (1)$$

where $n = 2$, H_0 is the nonrelativistic kinetic energy operator,

$$H_0 = -\frac{\Delta^{(2)}}{2M_b^0}, \quad (2)$$

and δH is the leading relativistic and finite-lattice-spacing correction,

$$\begin{aligned} \delta H = & -\frac{(\Delta^{(2)})^2}{8(M_b^0)^3} \left(1 + \frac{aM_b^0}{2n}\right) + \frac{a^2\Delta^{(4)}}{24M_b^0} \\ & -\frac{g}{2M_b^0} \boldsymbol{\sigma} \cdot \mathbf{B} + \frac{ig}{8(M_b^0)^2} (\boldsymbol{\Delta} \cdot \mathbf{E} - \mathbf{E} \cdot \boldsymbol{\Delta}) \\ & -\frac{g}{8(M_b^0)^2} \boldsymbol{\sigma} \cdot (\boldsymbol{\Delta} \times \mathbf{E} - \mathbf{E} \times \boldsymbol{\Delta}). \end{aligned} \quad (3)$$

Here $\boldsymbol{\Delta}$ and $\Delta^{(2)}$ are the simple gauge-covariant lattice derivative and laplacian, while $\Delta^{(4)}$ is a lattice version of the continuum operator $\sum D_i^4$. We used the standard cloverleaf operators for the chromo-electric and magnetic fields, \mathbf{E} and \mathbf{B} . The entire action was tadpole improved by dividing every link operator U_μ by $u_0 \equiv \langle \frac{1}{3} \text{Tr} U_{\text{plaq}} \rangle^{1/4}$. Potential models indicate that corrections beyond δH contribute only of order 5–10 MeV to Υ energies.

The only parameter in the NRQCD action is the bare mass of the quark, M_b^0 . We did a complete simulation for each of three masses: $2/a$, $1.8/a$, and $1.71/a$. Our analysis indicates that the last of these is the closest to the real mass (see below). However the statistical analysis for this mass is not yet complete and so most of the results we quote are for $aM_b^0 = 1.8$. Except where noted otherwise, the difference has negligible effect.

Note that meson energies in NRQCD are non-relativistic energies and do not include the rest mass energy. To obtain the rest mass of the Υ , for example, we measured the momentum dependence of its energy, fitting it to a form

$$E_\Upsilon(\mathbf{p}) = E_{\text{NR}}(\Upsilon) + \frac{\mathbf{p}^2}{2M_{\text{kin}}(\Upsilon)} + \dots \quad (4)$$

where the kinetic mass M_{kin} is the physical mass of the meson (see below).

Our quark propagators were computed using an ensemble of quenched configurations obtained from the Staggered Collaboration [5]. This ensemble contains $105 \cdot 16^3 \times 24$ configurations, generated with an unimproved Wilson action at $\beta = 6.0$ and gauge fixed to Coulomb gauge. Potential models indicate that the errors due to quenching and to finite- a errors in the gluon action could be order 40 MeV in Υ energies, making these the most important systematic errors.

We performed all of our measurements from 8 different origins separated by $L/2$ in the initial time slice, and treated the propagators at these origins as statistically independent. At each value of the bare mass, our spectrum measurements required a total of 17 heavy quark propagators, each with 3 spin-color components at the source and 6 at the sink, using about 17 GFlops-hour of CPU time, i.e. about 800 inversions per GFlops-hour.

When measuring meson propagators, we used gauge non-invariant smearing at both source and sink. With fast fourier transforms, all source-sink combinations can be measured at a computational cost of one quark-propagator inversion per source smearing function [6]. We used $1S$, $2S$, $3S$, $1P$, and $2P$ wavefunctions computed in the quark potential model (with the Richardson potential) as our smearing functions. In addition we used local sources for both S and P states. We also created smearing functions for S -states with small, nonzero momenta. For each allowed set of quantum numbers, all source-sink smearing combinations were measured, resulting in a 4×4 matrix of correlation functions for S states, 3×3 for P states, and 2×2 for momentum states.

3. Fitting

We used a variety of fitting strategies to obtain the spectrum from our meson propagators. For the spectrum of spin-averaged S and P states we tried two sorts of multiexponential fit to multiple propagators. In the first we fit multiple exponentials to the set of propagators with smeared sources and a local sink: for example, the ground and first excited state of the Υ were determined

by simultaneously fitting three exponentials to the $1l$ and $2l$ propagators, where $1l$ indicates $1S$ smearing at the source and local smearing at the sink, and $2l$ indicates $2S$ smearing at the source and local smearing at the sink. We discarded results from the highest energy state in such fits, since this is the most susceptible to biasing due to higher states. These are the propagators for which our statistics are the best; however, the statistical quality of the results degrades markedly for the excited states.

The second approach we used for spin-averaged spectra was to fit the full matrix of propagators formed by taking every combination of nonlocal smearing function at the source and at the sink: for example, the Υ and its first two excited states were determined by simultaneously fitting three exponentials to the 11, 12, 13, 21, 22, 23, 31, 32, and 33 propagators formed using quark-model wavefunctions for the first three S -states as smearing functions. The statistics were poorer for these smeared-smeared propagators compared with the smeared-local propagators discussed above; but the fitting is highly overdetermined, and consequently significantly more robust. This approach gave the best results for highly excited states; it also avoids spurious plateaus [7].

For splittings between two highly correlated states we found that the best method is to fit a single exponential to the jackknifed ratio of the two propagators for the two states. This approach is useful for computing spin splittings and the kinetic mass of the Υ .

Statistical uncertainties for the fitting parameters were estimated by varying the parameters until $\delta\chi^2 = 1$. In several cases we checked this estimate using a bootstrap analysis. The two estimates agreed in each case tested, suggesting that the statistical fluctuations in our propagators are at least approximately gaussian.

Our fitting protocol follows closely the techniques discussed in [8], including the use of singular value decomposition to allow the inversion of the variance matrix with finite precision arithmetic. In general, we had very few problems in obtaining successful fits, even for the second excited Υ state. This is due to the high statistics

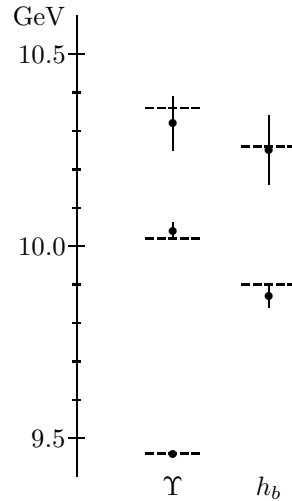


Figure 1. NRQCD simulation results for the spectrum of the $\Upsilon(^3S_1)$ and $h_b(^1P_1)$ and their radial excitations. Experimental values (dashed lines) are indicated for the S -states, and for the spin-average of the P -states. The energy zero for the simulation results is adjusted to give the correct mass to the Υ .

in our data set, and to our simultaneous fits using many smearing functions. In particular, it was important to include a smearing function for every state we were attempting to fit.

4. The Spectrum and a^{-1}

In Figure 1, we present our simulation results for the 3S_1 and 1P_1 spectra, together with the corresponding experimental values from [9]. We use $a^{-1} = 2.4$ GeV and Monte Carlo data with $aM_b^0 = 1.8$. Because the h_b has not been observed, the experimental values quoted for the 1P_1 states are actually the spin averages of the χ_b states; strong theoretical arguments, supported by our measurements, indicate that the two are the same.

In Figure 2, we present our results for the spin

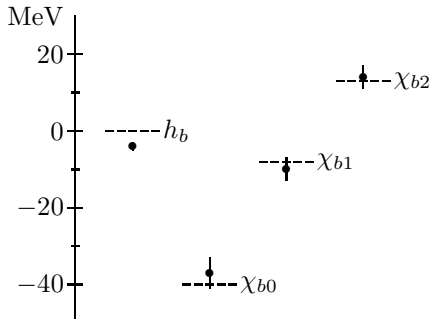


Figure 2. Simulation results for the spin structure of the lowest lying P -state in the Υ family. The dashed lines are the experimental values for the triplet states, and the experimental spin average of all states for the singlet (h_b).

splittings of the P -wave ground state. Again $a^{-1} = 2.4$ GeV and $aM_b^0 = 1.8$. The zero of energy is set to the spin average of the $\chi_b(1P)$. The error bars are only for statistical errors. We expect systematic errors in the P -state energies of order 5 MeV, which is comparable to the statistical errors shown.

We determined the inverse lattice spacing by fitting the simulated spectrum to the experimentally determined spectrum. Rather than choosing a^{-1} to make, say, the $\chi_b(1P) - \Upsilon(1S)$ splitting correct, we used a bootstrap analysis to perform a correlated fit for a^{-1} to the whole spectrum. Specifically, treating the 840 origins in our ensemble as statistically independent, we generated 20 bootstrap ensembles, each containing the meson propagators from 840 origins (with repetition). We then extracted the spectrum from each of these ensembles, giving us an ensemble of 20 spectra. Choosing various states for inclusion in the fit, we did a 1-parameter correlated fit of our spectra to the experimental spectrum to determine a^{-1} . This procedure was carried out twice, i.e. with two different sets of 20 bootstrap ensembles.

Splittings	a^{-1}	Q
$2S-1S, 1P-1S$	2.37(9)	.21
	2.41(10)	.42
$2S-1S, 1P-1S,$ $2P-1S$	2.42(7)	.27
	2.39(10)	.43
$2S-1S, 1P-1S,$ spin-splittings	2.32(6)	.15
	2.35(9)	.31

Table 1
Bootstrap results for a^{-1} .

The results of our a^{-1} fits for different groups of states are summarized in Table 1. The splittings for S -states are between 3S_1 states, while spin averages are used for the P -states. The spin-splittings used are for the lowest lying P -state. For each set of states fit, we tabulate the values of a^{-1} and the associated goodness of fit Q for both sets of 20 spectra. (Q typically lies between 0.1 and 0.9 for a good fit.) These fits indicate that

$$a^{-1} = 2.4(1) \text{ GeV}. \quad (5)$$

Because of quenching, our a^{-1} should not agree with those obtained by matching simulation results for observables that are more infrared, like the string tension, to experiment; we expect such determinations to yield smaller values of a^{-1} .

The success of our global fits of the Υ spectrum show that our simulation is accurately modeling the general features of the Υ physics. There are certainly systematic errors in our simulation results, but these do not degrade the fits because they are generally smaller than the statistical errors. Only a small improvement in statistics is needed before these systematic effects will become apparent. Indeed there is already a slight indication (2σ) that the $2S-1S$ and $1P-1S$ splittings are inconsistent, the first being too large and the second too small. This is precisely the effect expected due to quenching of the gauge fields. Such discrepancies will be useful when comparable simulations with unquenched configurations are begun. Similar effects are expected in the spin splittings, particularly for S -states.

β	aM_b^0	$aE_{\text{NR}}(\Upsilon)$	aE_0	M_b
6.0	1.71	0.455(1)	0.21	4.69
	1.80	0.451(1)	0.21	4.70
	2.00	0.444(1)	0.22	4.73

Table 2

Simulation and perturbative results used in the first method for determining M_b . Values for M_b are in GeV.

5. M_b determination

The b -quark's mass M_b is an important fundamental parameter of the Standard Model. Our simulation results lead to two independent determinations of this mass (ie, of the pole mass)[12]. These are among the most accurate and reliable of all determinations to date.

The first procedure for computing M_b uses simulation results for the nonrelativistic energy $E_{\text{NR}}(\Upsilon)$ of the Υ (Eq. (4)). The quark mass is given by

$$M_b = \frac{1}{2} (M_\Upsilon - a^{-1} (aE_{\text{NR}}(\Upsilon) - 2aE_0)), \quad (6)$$

where $M_\Upsilon = 9.46$ GeV is the experimentally measured mass of the Υ , and E_0 is the nonrelativistic energy of a $\mathbf{p} = 0$ b -quark in NRQCD. The quantity $E_{\text{NR}}(\Upsilon) - 2E_0$ can be thought of as the effective binding energy of the meson. The quark energy E_0 is an ultraviolet divergent quantity and thus it can be computed using weak-coupling perturbation theory [4]:

$$aE_0 = b_0 \alpha_V(q_0) (1 + \mathcal{O}(\alpha_V)) \quad (7)$$

Here α_V is the strong coupling constant as defined in [10], and $q_0 \sim 1/a$. In Table 2 we present the simulation results for E_{NR} , and the corresponding E_0 's from perturbation theory. From these results we conclude that the pole mass of the b -quark is $M_b = 4.7(1)$ GeV. The major source of uncertainty in this determination is from the two-loop corrections to E_0 . These could be 10–20% of E_0 , or 1–2% of M_b . Uncertainties due to finite lattice spacing, quenching, tuning of the bare quark mass, statistics, and a^{-1} are all less than 1%.

Our second procedure for determining M_b is

β	aM_b^0	$aM_{\text{kin}}(\Upsilon)$	Z_m	$M_{\text{kin}}(\Upsilon)$	M_b
6.0	1.71	3.95(5)	1.15	9.5(4)	4.72
	1.80	4.10(5)	1.15	9.8(4)	4.76
	2.00	4.45(5)	1.14	10.7(4)	4.82

Table 3

Simulation and perturbative results used in the second method for determining M_b . Values for $M_{\text{kin}}(\Upsilon)$ and M_b are in GeV.

to tune the bare quark mass M_b^0 until the kinetic mass of the Υ , as computed in the simulation (Eq. (4)), agrees with the measured mass of the Υ . Then the pole mass of the quark is $M_b = Z_m M_b^0$ where renormalization constant Z_m is computed using perturbation theory [4]:

$$Z_m = 1 + b_m \alpha_V(q_m) + \mathcal{O}(\alpha_V^2) \quad (8)$$

where scale $q_m \sim 1/a$. To reduce the sensitivity of the result to the value of the lattice spacing and to the bare quark mass, we rewrite the expression for the pole mass as

$$M_b = Z_m M_\Upsilon \frac{aM_b^0}{aM_{\text{kin}}(\Upsilon)} \quad (9)$$

where $M_\Upsilon = 9.46$ GeV is the Υ 's experimental mass, while $M_{\text{kin}}(\Upsilon)$ is its mass as determined from our simulation with bare mass M_b^0 . Our results are summarized in Table 3. These indicate that our best estimate for bare quark mass is $M_b^0 = 1.7(1)/a$, and therefore the pole mass is again $M_b = 4.7(1)$ GeV. Here the main source of uncertainty is again perturbative: the two-loop corrections to Z_m could shift M_b by 2–3%. Uncertainties due to a^{-1} , tuning the bare mass, etc. are of order 1% or less.

Our two determinations of the b -quark mass are very different, and yet they both yield a pole mass of $M_b = 4.7(1)$ GeV. The complete agreement between the two methods is a strong indication of the validity of each, and more generally of the lattice QCD techniques upon which they rely.

6. $\alpha_{\overline{\text{MS}}}(M_Z)$ Determination

The strong coupling constant is completely specified by two lattice quantities: the inverse

Loop	$\alpha_V(3.41/a)$
$\log W_{11}$	0.152
$\log W_{12}$	0.152
$\log W_{13}$	0.152
$\log W_{22}$	0.153
$\log W_{23}$	0.154
$\log W_{33}$	0.159

Table 4

The strong coupling constant as determined from Monte Carlo results for various Wilson loops.

lattice spacing a^{-1} , and the coupling at a scale $3.41/a$. The inverse lattice spacing has been discussed above. NRQCD simulations of the Υ system give $a^{-1} = 2.4(1)$ GeV, where the errors are dominated by statistics.

The coupling constant is obtained by fitting the Monte Carlo value of $\log\langle\frac{1}{3}\text{Tr}U_{\text{plaq}}\rangle$ to the perturbative expansion[10]

$$-\frac{4\pi}{3}\alpha_V(3.41/a)\{1 - 1.19\alpha_V\}. \quad (10)$$

This procedure, in effect, defines α_V . The reliability of perturbation theory can be assessed by computing α_V from a variety of Wilson loops, each with its own perturbative expansion (corrected to order α_V^3). We have done this and the results are shown in Table 4. Loops with small areas are less susceptible to nonperturbative effects and so we conclude that $\alpha_V^{(0)}(3.41/a) = 0.152(1)$.

Unfortunately we have $n_f = 0$ light-quark flavours in our simulation, while Υ physics is controlled by a theory with $n_f = 3$. Thus a correction is needed. The correction is illustrated by Figure 3 which shows plots of the running coupling constants for the $n_f = 0$ and $n_f = 3$ theories that give the same Υ physics. An $n_f = 0$ simulation gives $n_f = 3$ results at scale q^* if

$$\alpha_V^{(3)}(q^*) = \alpha_V^{(0)}(q^*). \quad (11)$$

For quarkonium the relevant q^* is the mean momentum-transfer in the potential, which is computed from the expectation value of the po-

tential between wavefunctions for the state of interest:

$$\langle\frac{\alpha_V^{(3)}(q)}{q^2}\rangle \equiv \alpha_V^{(3)}(q^*)\langle\frac{1}{q^2}\rangle. \quad (12)$$

Quark-model wavefunctions for $1s$, $2s$, and $1p$ states imply q^* is $0.75(25)$ GeV for Υ 's. To correct for the wrong n_f , we use the two-loop perturbative beta function to make the connections:

$$\begin{array}{ccc} \alpha_V^{(0)}(3.41/a) & & \alpha_V^{(3)}(3 \text{ GeV}) \\ \downarrow & & \uparrow \\ \alpha_V^{(0)}(q^*) & = & \alpha_V^{(3)}(q^*) \end{array} \quad (13)$$

The perturbative beta function is probably reliable down to scales of order 0.7–0.8 GeV (see Figure 3). We obtain a value for the unquenched coupling of

$$\alpha_V^{(3)}(3 \text{ GeV}) = 0.262(12) \quad (14)$$

where the uncertainty in q^* is the dominant source of error.

It is customary to quote values for the coupling constant in terms of $\alpha_{\overline{\text{MS}}}(M_Z)$. The standard $\overline{\text{MS}}$ coupling is related to α_V by

$$\alpha_{\overline{\text{MS}}}(q) = \alpha_V(e^{5/6}q)\{1 + 2\alpha_V/\pi + \mathcal{O}(\alpha_V^2)\}. \quad (15)$$

Converting to $\overline{\text{MS}}$ and running the scale up to the mass of the Z meson, we obtain finally:

$$\alpha_{\overline{\text{MS}}}^{(5)}(M_Z) = 0.112(4), \quad (16)$$

which compares well with other lattice determinations [11], as well as with 0.110–0.125 as obtained from various high-energy experiments. The main sources of error in our result are:

$$\begin{array}{lll} n_f = 0 \rightarrow 3 & \implies & 0.002 \\ \alpha_V \rightarrow \alpha_{\overline{\text{MS}}} & \implies & 0.002 \\ \alpha_V^{(0)}(3.41/a) & \implies & 0.001 \\ a^{-1} & \implies & 0.001 \end{array}$$

All of these errors can be significantly reduced in the immediate future.

7. Perturbative Improvement

The lowest-order (or Schrödinger) NRQCD action accounts for the bulk of Υ and ψ physics.

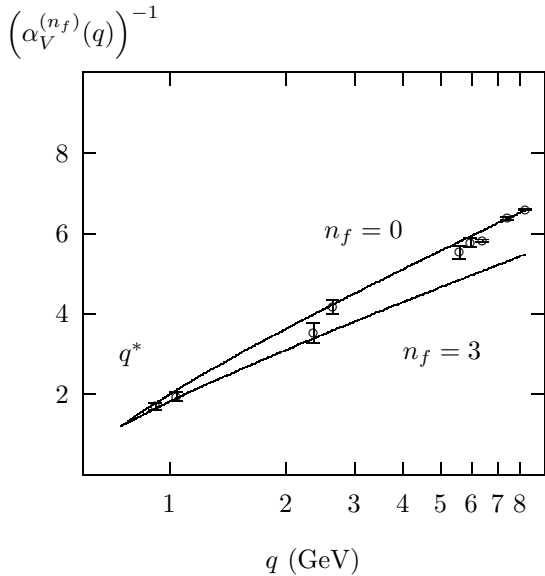


Figure 3. $(\alpha_V^{(n_f)}(q))^{-1}$ for the $n_f = 0$ and $n_f = 3$ theories having the same Υ physics. The two-loop perturbative beta function was used to generate the curves. The data points are values of $\alpha_V^{(0)}(q)$ determined from Monte Carlo measurements of various small Wilson loops and Creutz ratios of small loops. These show that two-loop perturbation theory is reliable over the entire range of q 's shown.

However high precision results require an improved action. The key ingredients for an improved action are:

- a tree-level perturbative calculation of the leading correction terms in the action (Eq. (3));
- tadpole improvement of the correction terms, where every link is replaced by

$$U_\mu \rightarrow U_\mu/u_0, \quad (17)$$

and u_0^4 is the Monte Carlo value of $\langle \frac{1}{3} \text{Tr} U_{\text{plaq}} \rangle$; this step is essential for avoid-

ing large renormalizations of the tree-level corrections;

- a calculation of $\mathcal{O}(\alpha_V(1/a))$ renormalizations of the corrections (if very high precision is needed).

We have implemented the first two of these improvements in our NRQCD simulations, and they have been strikingly successful, as is illustrated by the three examples listed in Table 5.

The first example is the determination of the Υ mass from its dispersion relation (Eq. (4)). This is compared with the “exact” result obtained from the relation

$$aM_\Upsilon = 2(Z_m aM_b^0 - aE_0) + aE_{\text{NR}}(\Upsilon), \quad (18)$$

where renormalizations Z_m and aE_0 are computed perturbatively, as discussed above (Eqs. (7) and (8)). Both the addition of correction terms to the action and tadpole improvement are essential for accurate results. The most important correction terms in the action for this quantity are the spin independent $\mathcal{O}(v^2, a, a^2)$ terms. (Note that the kinetic mass of a composite particle equals the sum of the masses of the constituents in a nonrelativistic theory; the binding energy comes in only with relativistic corrections.)

The second example is the spin-splitting between the χ_{b2} and χ_{b0} P -state in the Υ family. This splitting vanishes in the lowest order theory since that theory is spin independent. Tadpole improvement is essential here since the dominant operator that contributes to this splitting, $\psi^\dagger i\boldsymbol{\sigma} \cdot \mathbf{D} \times g\mathbf{E}\psi$, involves the cloverleaf operator for the chromoelectric field. Again only the fully corrected theory works well; it gives results in excellent agreement with experiment.

The third example is the spin-splitting between the ψ and η_c mesons [1]. The situation here is quite analogous to that for the P -state splittings, except that here the dominant operator is $\psi^\dagger \boldsymbol{\sigma} \cdot g\mathbf{B}\psi$. Again correction terms and tadpole improvement are essential. The fully corrected simulation gives an excellent result; the 20% discrepancy between this result and experiment is consistent with the expected size of α_V corrections, uncertainties in the mass, $\mathcal{O}(v^4)$ operators, and effects due to quenching.

Quantity	$\delta H = 0$	$u_0 = 1$	Corrected	Exact
aM_Υ	3.60(5)	5.00(5)	4.15(5)	4.10(9)
$\chi_{b2} - \chi_{b0}$	0	25(7)	51(7)	53 MeV
$\psi - \eta_c$	0		94(1)	117 MeV

Table 5

NRQCD predictions compared with exact results. Simulation results are presented for the theory without $\mathcal{O}(a, v)$ corrections ($\delta H = 0$), the theory without tadpole improvement ($u_0 = 1$), and for the fully corrected theory.

These results are compelling evidence that perturbative improvement of actions, when combined with tadpole-improved perturbation theory, is a highly effective procedure.

8. Conclusions

We have presented early results from our continuing program of high-precision analyses of heavy-quark mesons using NRQCD. We have shown that lattice simulations can accurately account for the structure of the Υ spectrum up through the $\Upsilon(3S)$, and including spin structure. And we have used these results to make new determinations of the strong coupling constant and the b -quark's mass.

Our results are possibly the most thorough QCD tests to date of perturbative improvement for lattice actions. They underscore the reliability of perturbation theory, the utility of tree-level improvement, and the critical importance of tadpole improvement (without it, the improvements tend to be much too small). The success of the perturbative improvement for NRQCD strongly suggests that it will work for gluons and light quarks, particularly since the quarkonium states we examine are 3–5 times smaller than light hadrons. (Note that $\mathcal{O}(a^2)$ errors for the Υ at $\beta = 6$ are only of order a few percent, even though the meson's radius is only two lattice spacings.) Simulations of light hadrons with improved actions should permit precision work on lattices that are much coarser than those commonly used today.

Acknowledgements

This work was supported in part by grants from the DOE, NSF, and SERC. The computer simulations were performed at the Ohio Supercomputer Center.

REFERENCES

- [1] C.T.H. Davies, these proceedings; and A.J. Lidsey, these proceedings.
- [2] G.P. Lepage and B.A. Thacker, Nucl. Phys. B (Proc. Suppl.) 4 (1988) 199; B.A. Thacker and G.P. Lepage, Phys. Rev. D43 (1991) 196.
- [3] G.P. Lepage, L. Magnea, C. Nakhleh, U. Magnea, and K. Hornbostel, Phys. Rev. D46 (1992) 4052.
- [4] C. Morningstar, these proceedings.
- [5] R. Gupta *et al*, Phys. Rev. D43 (1991) 2003.
- [6] A.X. El-Khadra, private communication.
- [7] C.T. Sachrajda, Nucl. Phys. B (Proc. Suppl.) 30 (1993) 20.
- [8] W.H. Press *et al*, *Numerical Recipes in C* (Cambridge University Press, Cambridge, 1992).
- [9] Particle Data Group: K. Hikasa *et al*, Phys. Rev. D45 (1992).
- [10] G.P. Lepage and P.B. Mackenzie, Phys. Rev. D48 (1993) 2250.
- [11] A.X. El-Khadra, these proceedings.
- [12] NRQCD Collaboration: C.T.H. Davies *et al*, submitted to Phys. Rev. Lett.